

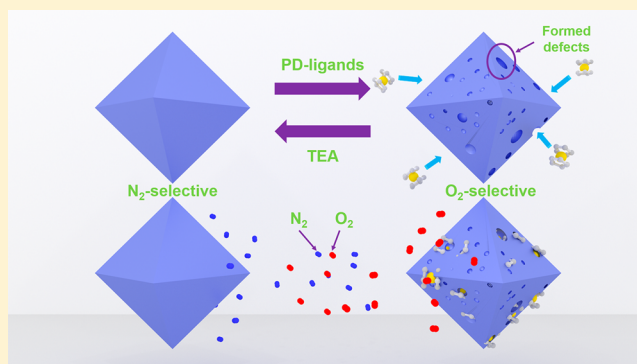
Investigation of Missing-Cluster Defects in UiO-66 and Ferrocene Deposition into Defect-Induced Cavities

Bohan Shan,[†] Sean M. McIntyre,[†] Mitchell R. Armstrong, Yuxia Shen, and Bin Mu^{*†}

Chemical Engineering, School for Engineering of Matter, Transport, and Energy, Arizona State University, 501 East Tyler Mall, Tempe, Arizona 85287, United States

Supporting Information

ABSTRACT: Advancing our understanding of the defect formation mechanism in metal–organic frameworks (MOFs) is critical for the rational design of the material's structure. In particular, the defects in the UiO-66 framework have been shown to have a significant impact on the framework functionality and stability. However, the effects of synthesis conditions on defect formation are elusive and our understanding of missing-ligand and missing-cluster defects in UiO-66 is far from clear. In this work, we demonstrate that the formation of missing-cluster (MC) defects is due to the large number of partially deprotonated ligands in synthesis solution. The proposed mechanism is verified by a series of syntheses controlling the defect formation. The results show that the quantity of MC defects is sensitive to deprotonation reagents, synthesis temperature, and reactant concentration. The pore size distribution derived from the N₂ adsorption isotherm at 77 K allows accurate and convenient characterization of the defects in UiO-66. The existence of defects in the UiO-66 framework can cause significant deviations in its pore size distribution from the results derived from the theoretically perfect crystal structure. The extra cavities generated by MC defects are demonstrated to allow deposition of a large functional molecule, ferrocene (3.5 Å × 4.5 Å × 4.5 Å). The successful incorporation is proven by the tuning of the original N₂-selective framework to become an O₂-selective framework.



1. INTRODUCTION

Metal–organic frameworks (MOFs) are porous materials consisting of metal nodes linked by organic ligands. Due to their intriguing pore structures and functionalities, these materials are given much consideration for applications in separation,^{1,2} energy storage,^{3,4} catalysis,⁵ and sensing.^{6,7} However, due to the nature of the coordination bond, many of the reported MOFs have undesirable stability.⁸ The synthesis of UiO-66, a highly coordinated ZrMOF, is one of the significant efforts made to enhance the stability of MOFs.^{9–11} From a thermodynamic perspective, high valence state Zr⁴⁺ can form a strong coordination bond with the ligand.^{12–14} Different from the soft Lewis acids such as Cu²⁺ and Zn²⁺, the Zr⁴⁺ cluster is a hard Lewis acid that can form a stronger coordination bond with the hard Lewis base carboxylates.¹⁵ The high coordination number of Zr also increases the steric hindrance of the Zr–ligand connection area and the tolerance for external impact.¹⁶

However, the high stability of UiO-66 increases the inertness of the framework as well, which could be a drawback for selective adsorption and catalysis.¹⁷ Therefore, the defective UiO-66 has become an attractive option due to its highly reactivated framework. Zhou et al. reported a systematic study of acetic acid modulated defective UiO-66, in which the

surface area dramatically increased because of the defects.¹⁸ Zhong et al. reported the synthesis of defective UiO-66 modulated with benzoic acid. The synthesized sample has a surface area as high as 1890 m²/g, much higher than the theoretical surface area around 1200 m²/g.^{19,20} As a result of the increased surface area and different compensating groups, the defects can effectively modify the adsorption properties of synthesized UiO-66. The CO₂ adsorption capacity is strongly influenced by the defects and various compensating groups.^{18,21} The hydroxylated form of UiO-66 has a higher CO₂ heat of adsorption (28 kJ/mol) compared to the dehydroxylated form (22 kJ/mol). The OH–O columbic interaction is attributed to this enhanced heat of adsorption.¹⁸ In addition, Dirk E. De Vos and co-workers reported the study of trifluoroacetate and hydrochloric acid modulated UiO-66 synthesis.²² The open metal sites created by removing the compensating groups are attributed to their increased catalytic activity. Furthermore, the substitution of compensating groups

Received: July 27, 2018

Revised: September 7, 2018

Accepted: September 26, 2018

Published: September 26, 2018

with more reactive groups opens an avenue for triggering the framework activity using easy and inexpensive methods.¹⁷

The outstanding stability is the major reason that UiO-66 is prominent among MOFs. This feature pushes it closer to practical applications than most MOFs. While we are excited that the defective frameworks can dramatically enhance the UiO-66 activity, the defects could also negatively impact its stability. Despite the extraordinary properties that “defects” have brought to us, some efforts have been made to reveal what these defects have taken from us. The water adsorption in defective UiO-66 is highly enhanced.¹⁹ The framework shifted sharply to hydrophilic by the introduction of defects. The heat of adsorption at low loading increases from ~ 15 kJ/mol of ideal unit cell to 60–70 kJ/mol of defective unit cell. UiO-66 synthesized at low temperature (100 °C) shows a significant number of defects, and the framework collapses under heat treatment at 250 °C. Meanwhile, the nondefective framework remains stable until 400 °C.²³ The chemical stability of UiO-66(Hf) was tested by Goodwin and co-workers. Even though the framework did not fully collapse, the crystallinity significantly decreased under exposure to water, HCl, NaOH, and methanol.²⁴ Therefore, the control over defect formation in the UiO-66 framework is extremely important for the advanced development of this material. It is meaningful to investigate the framework formation mechanism and relationship between reactants to direct the rational synthesis design.

In this work, we reaccommodate the existing mechanism of the defect formation process by taking the deprotonation step into account. We propose the existing coordination modulation mechanism can describe the missing-ligand (ML) defect formation, but the missing-cluster (MC) defect formation is due to the partially deprotonated ligands (PD-ligands) surrounding particles caused by the accumulated protons during synthesis. This hypothesis can explain why the defects increase dramatically with decreasing pK_a values of modulators. A series of syntheses and characterizations were carried out to verify this hypothesis. These results will be important for advancing our understanding of the defect formation process. Although much of the excitement around defect engineering in UiO-66 has focused on the reactivation of the framework based on ML defects for CO₂ adsorption, the systematic introduction of defects in the highly stable Zr-MOF could have broader applications. To emphasize this, a UiO-66–Ferrocene composite was synthesized by immobilizing ferrocene molecules within the generated void space from MC defects. Ferrocene was used as a probe molecule to demonstrate how the porosity from MC defects leads to drastically increased accessibility of framework for doping of large function molecules or precursors.²⁵ The successful incorporation of the redox-active ferrocene molecules was characterized by enhanced selectivity of the material toward oxygen.

2. EXPERIMENTAL MATERIALS AND METHODS

2.1. Chemicals. All the chemicals were purchased from commercial vendors and used as received without any further purification. Zirconium chloride (ZrCl₄), terephthalic acid (H₂BDC), formic acid (FA), acetic acid (AA), and ferrocene were purchased from Sigma-Aldrich. *N,N*-Dimethylformamide (DMF) and acetone were purchased from Fisher Scientific, and triethylamine (TEA) was purchased from Alfa Aesar.

2.2. Synthesis. ZrCl₄ (1.5 mmol) and H₂BDC (1.5 mmol) were dissolved in 30 mL of DMF with varying amounts of acetic acid or formic acid added. The modulator:ligand molar

ratios used are 25:1, 50:1, 100:1, and 150:1. The mixed solution was poured in a Teflon lined stainless steel reactor and heated at 120 °C for 24 h.

The UiO-66-FA-100 °C sample was synthesized at 100 °C and used the same procedure as previous samples. The UiO-66-1/3C samples were synthesized by dissolving ZrCl₄ (0.5 mmol) and H₂BDC (0.5 mmol) in 30 mL DMF with modulator:ligand molar ratio at 100:1. The UiO-66-TEA samples were synthesized using the same procedure with the addition of TEA at 0.16 mL (TEA-1) and 1.06 mL (TEA-2).

2.3. Computational Study. The nondefective UiO-66 framework structure information was taken from Lillerud and co-workers' results¹⁰ and uploaded into the RASPA molecular software package developed by Dubbeldam et al.²⁶ The UiO-66 frameworks with ML defects and MC defects are generated from the original nondefective structure using Mercury, and the corresponding cif files were uploaded into RASPA. The simulation box dimension was 42 Å × 42 Å × 42 Å with cutoff distance at 12 Å. In each simulation, 1×10^4 cycles were used (when increasing cycles, the results remain unchanged). The pore size distribution was calculated geometrically, where the pore size at a particular location was represented by the largest sphere that can fill the voids but not overlap with any framework atoms.^{27,28} The pore size distribution is calculated by the Monte Carlo volume integration.

3. RESULTS AND DISCUSSION

3.1. Mechanism of Missing-Cluster Defect Formation.

As proposed in the previous section, we attribute the formation of MC defects to the PD ligands, which is caused by the large number of protons in synthesis solution. In UiO-66 synthesis, the strong Zr-BDC interaction leads to a high activation energy and small rate constant of dissociation. The insufficient structure reorganization and defect reparation is the reason for the formation of a gel-like product commonly seen in MOF synthesis. Hence, the addition of a modulator has become an effective method to produce highly crystalline samples.²⁹ The coordination modulation effect is understood from two perspectives: (1) the competitive coordination between modulator and ligand kinetically brings the reaction rate of ligand dissociation to the equivalent level of ligand association. Therefore, the synthesized sample has enough structural reorganization and reparation to achieve a highly crystalline product. Additionally, when the Zr-ligand reaction rate is lowered, the number of formed nuclei decreases and each formed nucleus can grow larger. (2) The coordination reaction direction depends on the amount of added modulator. The competitive coordination between ligand-Zr and modulator-Zr can thermodynamically cause the reaction equilibrium to shift in the reverse direction. When “excessive” modulator is added, the Gibbs energy of the forward reaction becomes larger than zero and the reaction ends as a clear solution. Between the kinetically controlled crystallinity improvement and thermodynamically controlled complete coordination equilibrium shift, the coordination equilibrium can potentially lead to the crystal morphology variation of the synthesized sample.^{30,31}

The modulation effect in controlling the UiO-66 morphology is not as obvious as reported in other MOFs. This may be attributed to the high coordination number of Zr diminishing the variation caused by modulator. Instead, under the addition of modulator, people observed the defect formation inside a UiO-66 crystal rather than a crystal morphology change. The view that the defects are formed due to the thermodynamic

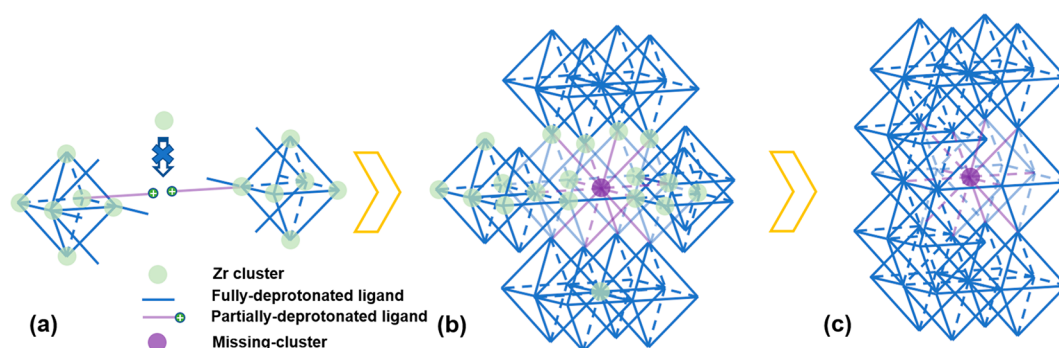


Figure 1. Diagram of partially deprotonated ligands (purple) that promote the missing cluster defect.

coordination equilibrium shift does not work well. Studies have shown defects in UiO-66 are highly dependent on the acidity and concentration of modulator.³² The addition of modulator with low pK_a value leads to a larger amount of defects (evident from dramatically increased surface area). Modulators with higher pK_a value can form a stronger bond with Zr clusters. If defects were caused by coordination equilibrium shift, a higher pK_a modulator could lead to more defects than modulator that has a smaller pK_a value. However, the opposite has been observed. Furthermore, Goodwin et al. investigated the defective UiO-66(Hf) framework.²⁴ The FA modulated UiO-66(Hf) contains two types of defects: ML defects and MC defects. If the defect formation is a thermodynamically driven process, the modulator would attack the clusters coordinated with more ligands and these defects would be well-dispersed through the entire framework. The MC defects inside the crystal are concentrated in a nanoregion instead of being well-dispersed throughout the entire crystal, indicating the situation is more complicated than the coordination equilibrium shift. The coordination equilibrium mechanism can describe the coexistence of Zr-modulator coordination and Zr-ligand coordination. Meanwhile, the MC defects are caused by the PD-ligands surrounding particles because the PD-ligands can only coordinate with one Zr cluster. The common M:L molar ratio used in UiO-66 synthesis can vary from 20 to 100. However, when we discuss the importance of M:L molar ratio, we automatically assume they are fully deprotonated and ready to react with Zr. But we should treat modulator as $H_n[\text{Modulator}]$ and ligand as $H_n[\text{Ligand}]$; the competitive relationship is between the $[\text{Modulator}]$ and $[\text{Ligand}]$. The $(n + 1)$ protons should also be taken into account. In this work, we reaccommodate the existing mechanism by taking into account the deprotonation step.

As shown in Figure 1, when two clusters approach each other, the PD-ligands at the particle surface cannot connect by accepting a Zr cluster in between them. Meanwhile, the particle surface covered by fully deprotonated ligands can still grow with adjacent particles. This model can explain why the defects increase dramatically with decreasing pK_a values of added modulators. Since modulators with lower pK_a value deprotonate easier, there will be a larger number of protons in the synthesis solution, which can suppress ligand deprotonation. Therefore, the reasoning is that the more modulator or the lower the pK_a value (higher acidity) of the modulator, the more protons exist in the synthesis solution. These protons increase the difficulty of ligand deprotonation, so more MC defects are formed. Considering the defect formation in an adjacent manner, PD-ligands may exist from the beginning, but

not in a high quantity because ligands have not started to coordinate with Zr clusters. Therefore, the chance of a nucleus meeting with PD-ligands is low at the initial stage of synthesis. This chance rises as the reaction proceeds.

3.2. Characterization of Missing-Ligand and Missing-Cluster Defects. To further verify our hypothesis that the formation of MC defects is a result of accumulated PD-ligands, a series of UiO-66 samples were synthesized under FA or AA modulation with varying synthesis conditions. Figure 2(a)

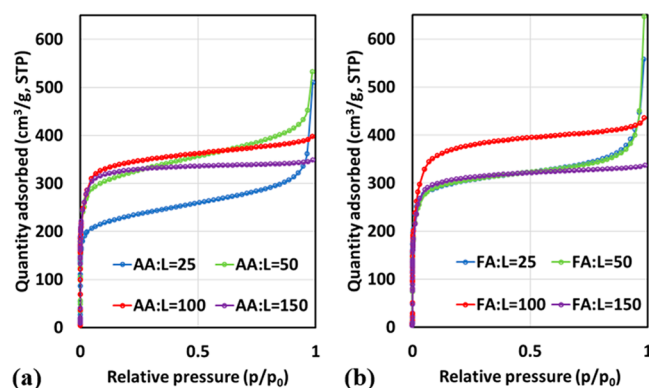


Figure 2. N_2 adsorption isotherms of UiO-66 synthesized with AA:L and FA:L ratio varying from 25 to 100.

shows the N_2 adsorption isotherms of a series of UiO-66 samples synthesized with varying acetic acid:ligand (AA:L) molar ratios. When AA:L ratio increases from 25 to 100, the surface area increases from 860 m^2/g to 1302 m^2/g . In comparison to the theoretical surface area of UiO-66, 1200 m^2/g , this observation indicates that the reaction product transformed from a partially crystalline gel-like sample to a crystalline defective framework. The FA modulated samples follow the same trend. In addition, at the same molar ratio of metal to ligand (M:L), UiO-66-FA shows a higher surface area. This result is consistent with those reported by Lillerud et al., and the improved crystallinity (Figure S2) can be explained by the kinetic model.^{15,32} However, when the M:L molar ratio is further increased from 100 to 150, the surface area of synthesized samples starts to decrease instead of continuing to increase. The surface areas of both samples are still higher than the theoretical value. We attributed this observation to extra protons in the synthesis solution stabilizing the formed Zr metal clusters, decreasing the formation of MC defects.³³

Based on the thermogravimetric analyses of UiO-66-FA/AAs (Figure 3), the weight loss starting after 450 $^{\circ}C$ is assigned to the BDC dissociation.³² The residual weights are

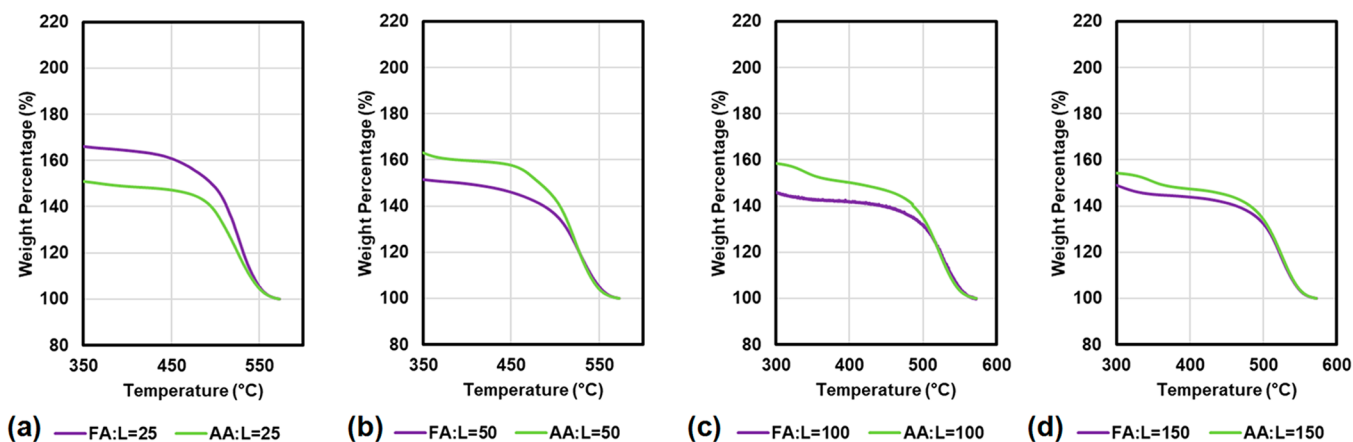


Figure 3. TGA patterns of UiO-66 synthesized with varying AA:L and FA:L molar ratios.

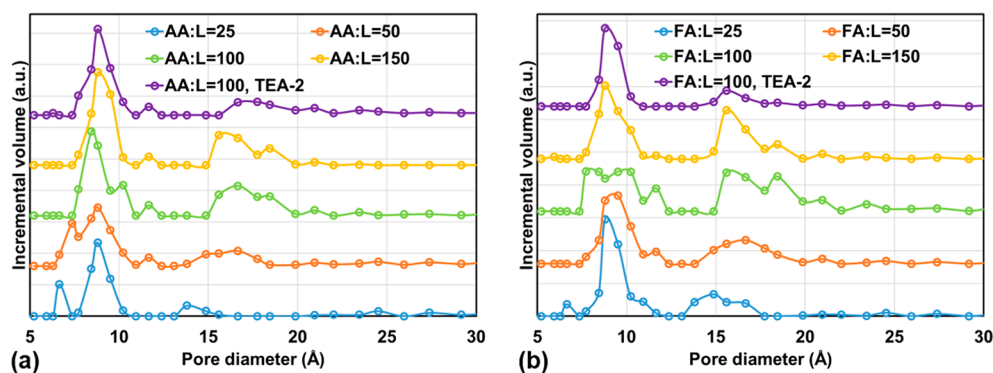


Figure 4. Experimental pore size distribution of UiO-66 synthesized with varying M:L molar ratio and TEA.

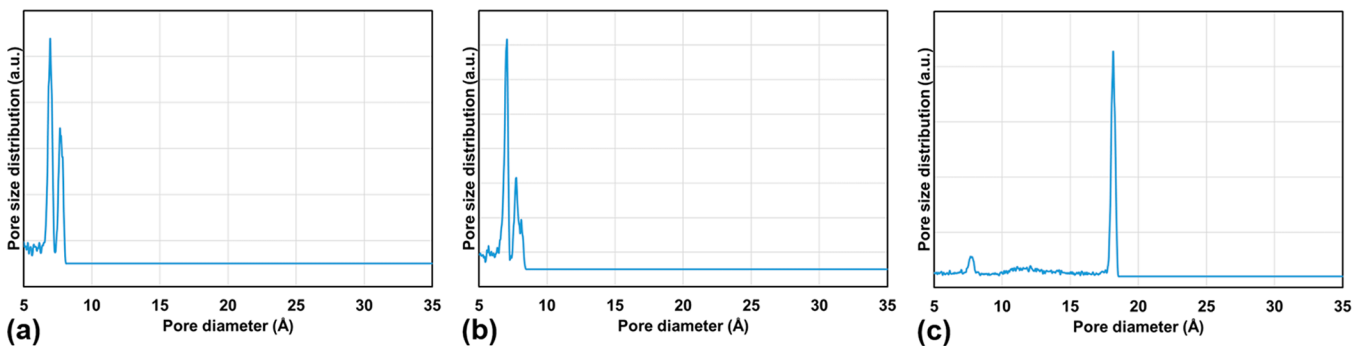


Figure 5. Simulated pore size distributions of (a) UiO-66 framework and (b) UiO-66 framework with ML defects and (c) UiO-66 framework with MC defects.

adjusted to the same level to show the relative amount of BDC, in which the MC defects in the unit cell were ignored. In Figure 3a, the plateau height of UiO-66-AA is smaller than the one of UiO-66-FA, indicating it has more ML defects than UiO-66-FA. The higher pK_a value of AA compared to FA increases the number of Zr-AA bonds, which become ML defects in the framework. When the M:L ratio is further increased (Figure 3b–d), the protonation suppression effect of FA increases the ML defects in UiO-66-FA samples. Therefore, the UiO-66-FA samples are shown to have more ML defects than UiO-66-AAs under TGA. In Figure 3d, consistent with the BET results, the difference between UiO-66-FA and UiO-66-AA TGA curves becomes smaller with higher M:L ratio. This observation may be attributed to the decreasing number of MC defects since a large number of ML defects were

contributed from the MC regions. However, this characterization method has some limitation in differentiating the type of defects because we manually ignore the MC defects in residue mass to back-calculate the number of missing ligands.

The pore size distribution analysis has been performed on those UiO-66-FA and UiO-66-AA samples (Figure 4). The pore size distribution of UiO-66-AA-25 has a peak positioned at ~ 6.6 Å and a slightly broader peak ranging from 7.7 to 10 Å, centered at ~ 8 Å. Along with the increase of modulator quantity, the peak at ~ 6 Å gradually merges into the bigger pore peak and a new peak starts to show up between 15 and 20 Å. To gain additional insights into these results, the simulated pore size distribution of the nondefective UiO-66 framework, calculated by the RASPA package, is presented in Figure 5a as a comparison. The simulated result shows two major peaks at

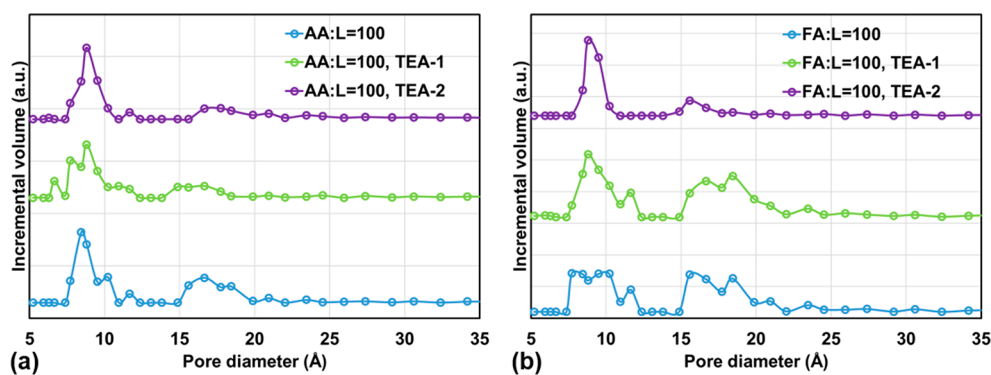


Figure 6. Pore size distribution of sample synthesized with varying amount of TEA added.

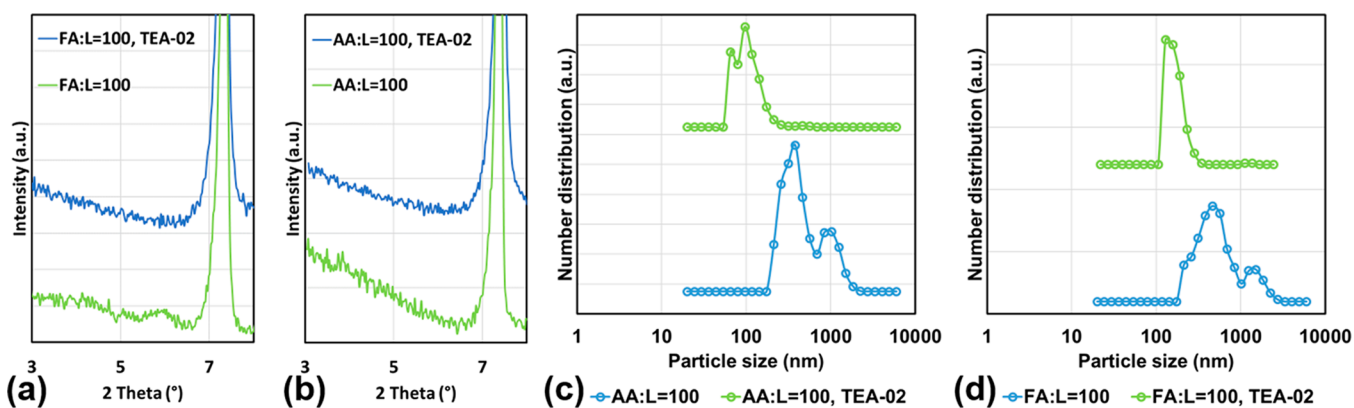


Figure 7. PXRD patterns of UiO-66 synthesized with and without TEA modulated with (a) FA and (b) AA. Particle size distribution of UiO-66 particles synthesized with and without TEA using (c) AA and (d) FA.

6.9 and 7.7 Å. The simulation results from the nondefective UiO-66 framework are mostly consistent with the pore size distribution results derived from N₂ adsorption isotherms. In Figure 5b, four ligands coordinated with one Zr cluster are removed in a unit cell. The simulated results of this framework show one peak shift from 6.9 to 7.1 Å, and another peak at 7.7 Å becomes broader due to the new peak coming out at 8.1 Å. Therefore, it is reasonable to expect if more ligands are disassociated from Zr clusters, the pore size distribution peaks will shift to larger diameters. In the experimental pore size distribution data (Figure 4), the peak at 6.6 Å merging into the broad peak position at ~8 Å can be attributed to the ML defects when an increasing amount of modulators is added. Meanwhile, the appearance of ML defects spans the entire framework, indicating the formation of ML defects is a thermodynamically driven process. It can then be concluded that the pore size distributions derived from N₂ adsorption isotherms adequately reflect the real situation. In addition, when the M:L molar ratio reaches 25 or higher, the ML defects can severely change the pore size of the UiO-66 framework from what is understood from its crystal structure. This observation is critical because when MOFs synthesized under modulation coordination are applied to adsorptive separation or membrane separation, the pore size plays an important role in determining the separation efficiency. In Figure 4, another important peak between 15 and 20 Å is not shown in either Figure 5a or Figure 5b. To understand these cavities, the simulated pore size distribution of a defective UiO-66 framework with one metal cluster removed from one unit cell is shown in Figure 5c. The two peaks at small diameters significantly decreased and a new peak between 15 Å to 20 Å

appears. This makes it clear that the new peak observed in Figure 4 is caused by MC defects. The peaks in experimental results are broader than the simulated result because of the missing-cluster defects that appear together in an adjacent manner as reported by Goodwin and co-workers.²⁴ As modulator concentration increases, the peak representing the MC defects increases. Under the addition of AA and FA, the UiO-66 framework contains a large number of pores that are larger than 1 nm and close to mesopores, due to the large amount of MC defects. The significant difference between ML defects peak and MC defects peak indicates these two types of defects are distinguishable and are formed based on different mechanisms. As reported, when the same amount of modulator is added in the synthesis, modulator with lower pK_a value leads to a higher surface area.³² In Figure 4, at the same M:L molar ratio, the pore size distribution peak, representing MC defects of UiO-66-FA, is much higher than the one of UiO-66-AA. This observation suggests that the higher surface area of UiO-66 synthesized with low pK_a value modulators is caused by increasing MC defects. This is because the lower pK_a value modulator has stronger deprotonation capability, leading to accumulation of protons in the synthesis solution. The larger number of accumulated protons leads to more PD-ligands. Consistent with the adsorption data, when the M:L ratio increased to 150, the peak height representing MC defects decreases, indicating that fewer MC defects are formed.

3.3. Effects of Deprotonation Reagent, Temperature, and Concentration. Our hypothesis that the MC defects are caused by the PD-ligands is slightly different from the discussion presented by Lillerud et al., in which the MC

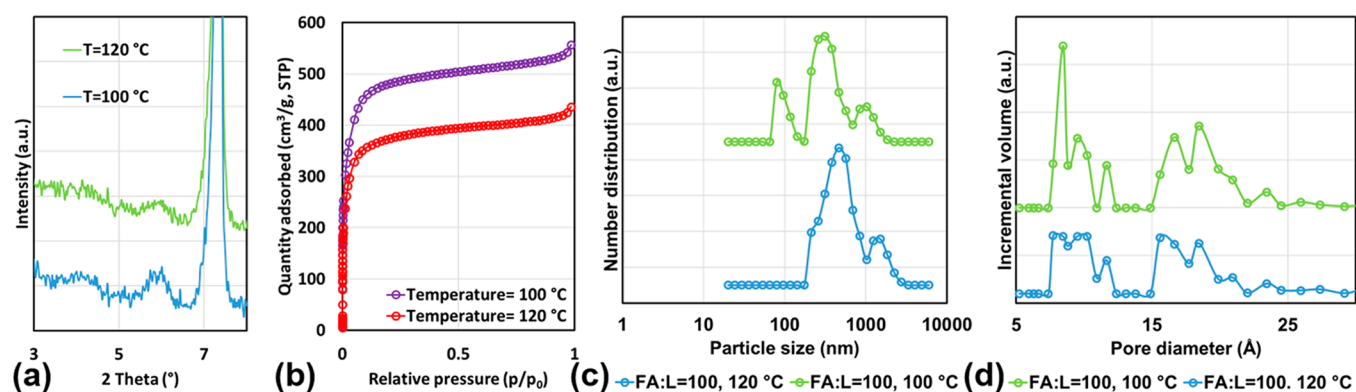


Figure 8. (a) PXRD patterns, (b) N_2 adsorption isotherms, (c) particle size distributions, and (d) pore size distributions of UiO-66 synthesized at different temperatures.

defects were formed due to the deprotonated modulator coordinating onto Zr clusters and remaining there until the end of the reaction.³² They proposed that the lower pK_a value of FA (higher acidity) causes more formate in the solution and the actual formate:deprotonated ligand ratio is higher than the acetate:deprotonated ligand ratio at the same M:L molar ratio. Contradictory to this opinion, the common understanding of the Zr–modulator coordination bond is that modulator with higher acidity forms a weaker Zr–modulator bond.³⁴ The presented data is inconsistent with this view because the Zr–formate interaction is weaker than the Zr–acetate interaction since formic acid has a lower pK_a value. Therefore, the conclusion that the coordinated modulator is the reason for MC defect formation is unjustified. As we presented above, from the pore size distribution data derived from N_2 adsorption isotherms, we can accurately track the ML defects and MC defects formed in UiO-66 synthesis. To further verify the role of the PD-ligands, we employed the deprotonation reagent, TEA, in the synthesis with M:L molar ratio = 100. Usually, the deprotonation reagents are alkaline and their function is promoting the reaction between metals and ligands in MOF synthesis.^{35,36} In Figure 6, for both UiO-66-FA and UiO-66-AA, after the addition of TEA, the pore size distribution peak representing MC defects is significantly decreased. In addition, as seen in Figure 7a and b, when TEA is added in the synthesis solution, the height of the peak representing the defects in PXRD patterns significantly decreased for both FA modulated synthesis and AA modulated synthesis. When deprotonation reagent is added in synthesis solution, it can facilitate the deprotonation of ligands and, therefore, decrease the number of PD-ligands. Hence, the number of MC defects is significantly decreased. If the MC defects are caused by the modulator capping effect as described by Lillerud et al., we should not see a significant decrease of MC defects since the addition of TEA will not impact the Zr–modulator interactions. This observation supports the mechanism that PD-ligands cause the MC defects.

In Figure S3, the particle size distributions of synthesized samples are measured by dynamic light scattering (DLS). The same as reported previously, modulator increased the particle size of synthesized UiO-66 crystals. When the M:L molar ratio increased, the modulation effect slowed down the nucleation process and allowed for crystal particles to grow to a larger size. Meanwhile, the particle size of UiO-66 became less uniform. We suggest that the particle size distributions can be explained in terms of the crystallization mechanism. The crystallization

rate of UiO-66 can be limited by the rate of nucleation or the rate of growth. As the number of protons (i.e., the modulator concentration) in the synthesis solution is increased, the crystallization process switches from being growth-rate-limited to nucleation-rate-limited, leading to larger, heterogeneous particle sizes.^{37,38} Consistent with this hypothesis, the nucleation process was proposed to be the rate-limiting step in the modulated synthesis of Zr-fumarate, indicated by its higher activation energy.^{33,37} The study also reported increasing particle size with the addition of modulator. Meanwhile, in the synthesis of UiO-66 with addition of HCl, the nucleation activation energy is lower than the one of growth.³³ The size of the synthesized crystal particles, in this case, is decreased under the addition of HCl. As seen in Figure 7(c) and 7(d), when TEA is added into the synthesis solution, the particle size distributions of UiO-66 synthesized with both FA and AA become much more uniform and the particle size decreases. The observation is consistent with the result reported by Lu et al., but we suggest the mechanism described above is responsible for this behavior.³⁹ The decrease in particle size and uniformity of particle size distribution is caused by the TEA largely decreasing the proton concentration, which promotes nucleation and results in a growth-limited crystallization process. The same trend has been observed under the addition of water in synthesis.³³

Reaction temperature also influences the quantity of PD-ligands produced in the reaction solution. In Figure 8, UiO-66 samples were synthesized at 100 and 120 °C with FA:BDC molar ratio set to 100. The UiO-66-FA synthesized at 100 °C shows a higher defect peak in PXRD patterns and higher N_2 adsorption capacity compared with the one synthesized at 120 °C (Figure 8). The surface area of UiO-66-FA-100 °C is around 1800 m^2/g , which is one of the highest reported surface areas of UiO-66. Compared with the sample synthesized at 100 °C, the UiO-66-FA-120 °C has lower surface area (1500 m^2/g). It has been reported that the synthesis of UiO-66 at 220 °C can produce a relatively defective-free framework.²³ Meanwhile, the particle size distribution of UiO-66-FA-120 °C is slightly more uniform compared with UiO-66-FA-100 °C (Figure 8c). Therefore, when the samples are synthesized at the same M:L molar ratio, the amount of MC defects is sensitive to the synthesis temperature. Based on our hypothesis, when the synthesis temperature is decreased, lower synthesis temperature can result in more PD-ligands since deprotonation is an endothermic process. This explains previous observations of less defectivity at higher temperature.

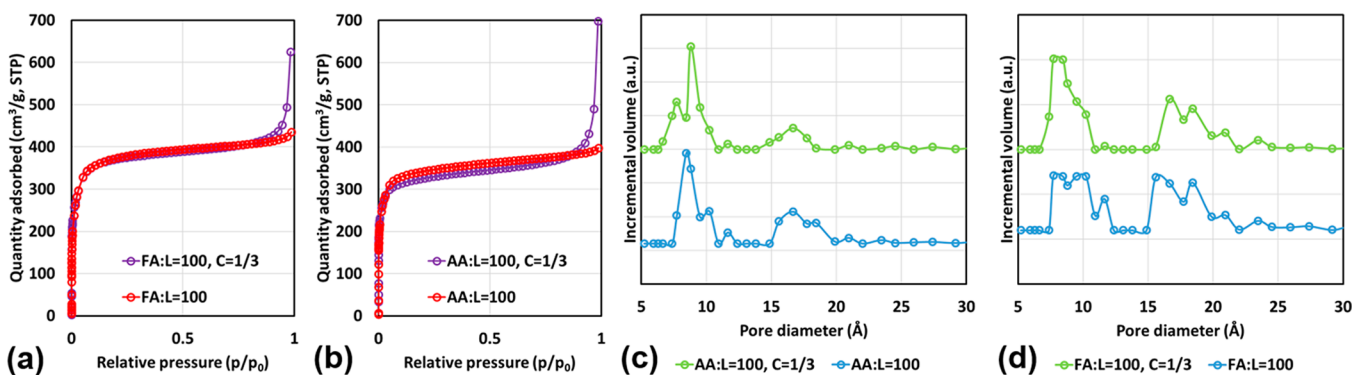


Figure 9. N_2 adsorption isotherms of UiO-66 and pore size distributions of UiO-66 synthesized at the original concentration (FA:L = 100) and 1/3 of the original concentration (FA:L=100, C = 1/3).

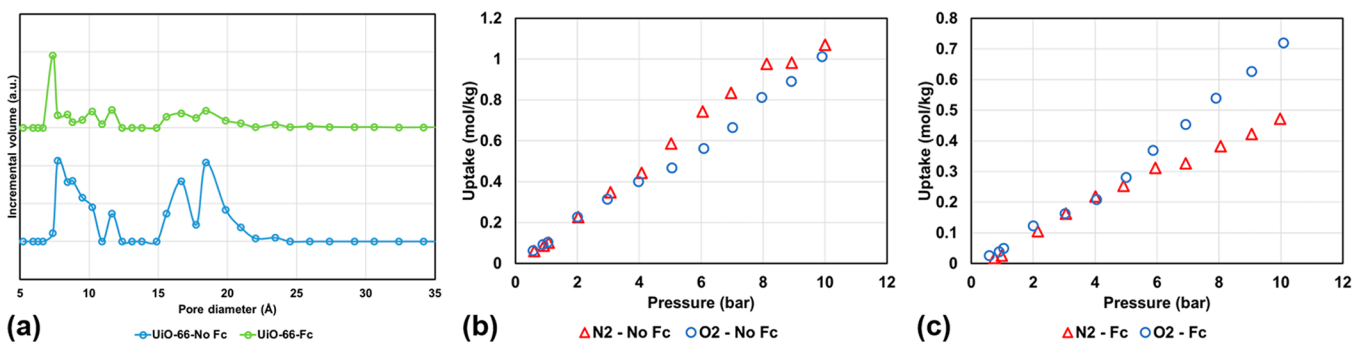


Figure 10. (a) Pore size distributions of UiO-66 with (UiO-66-Fc) and without (UiO-66-No Fc) ferrocene. N_2 and O_2 adsorption over (b) UiO-66 and (c) ferrocene modified UiO-66.

To confirm the increased number of defects is a result from more PD-ligands at lowered synthesis temperature, we again added deprotonation reagent in the synthesis. When TEA is added into the synthesis solution (100 °C), the particle size distribution became more uniform and the pore size distribution peak representing the missing cluster defects significantly decreased (Figure S4). Another important parameter that matters for the partial deprotonation mechanism is the reactant concentration. With the molar ratio among reactants remaining constant, the concentration variation of reactants will not severely impact the reaction equilibrium but will impact the proton concentration in the system. To further evaluate the effect of proton concentration, a UiO-66 sample was synthesized with the molar ratio between reactants held constant, but the reactant concentrations were reduced to 1/3 of the original concentrations. In Figure 9, the pore size distribution and N_2 adsorption isotherms of UiO-66 (Modulator:L = 100, 1/3) are shown. For both AA and FA modulated UiO-66s, the reduced reactant concentration decreases the samples' surface areas. Meanwhile, the pore size distribution peak representing the missing-cluster defects also decreased along with decreasing reactant concentrations. Therefore, the observation that the amount of MC defects is sensitive to the reactant concentration is aligned with our partial deprotonation mechanism for MC defect formation.

3.4. Ferrocene Deposition into MC Defect-Induced Cavities. MC defects create large pores in the UiO-66 framework, in which we can deposit molecules to change the functionality of UiO-66. Here, ferrocene, a widely used probing molecule, was deposited into the UiO-66 framework via the chemical vapor deposition (CVD) method. The UiO-66 and the ferrocene-functionalized UiO-66 (UiO-66-Fc) were

characterized using BET surface area measurements and pore size distribution measurements. Before the CVD process, the UiO-66 sample had a BET surface area of 1714 m^2/g . After loading, the surface area was reduced to 703 m^2/g due to ferrocene deposition. The pore size distributions of the UiO-66 and UiO-66-Fc (Figure 10) show a 5-fold reduction in the peak associated with the MC defects between 15 and 20 Å, indicating that most ferrocene molecules are deposited into the MC defective sites of the framework. This result reveals the extra cavities generated by the MC defects are accessible sites for functional molecules deposition. Pure oxygen and nitrogen adsorption isotherms were collected up to 10 bar at 40 °C on both UiO-66 and UiO-66-Fc samples. As shown in Figure 10, the original UiO-66 sample is essentially inert with a slight preference for nitrogen.⁴⁰ The uptake of the ferrocene-loaded sample is decreased substantially because of the decreased surface area. There is an increase in selectivity toward oxygen in the composite material at high pressure; at 10 bar, the selectivity is increased from 1.01 in the original sample to 1.51 in the ferrocene-loaded sample. The deposition of oxygen-scavenging ferrocene molecules in MOFs has been used to achieve enhanced O_2 selectivity, and the variation in the O_2/N_2 adsorption over UiO-66 after CVD process indicates the existence of ferrocene molecules.⁴¹

4. CONCLUSION

In this work, we presented the discussion of a defect formation mechanism in the UiO-66 framework. The coordination equilibrium shift under the addition of modulator can cause the formation of ML defects. Alternatively, the MC defects are caused by the PD-ligands as a result of the accumulated protons in synthesis solution. A series of experiments were

designed to verify the proposed mechanism so that we can demonstrate that the formation of MC defects is sensitive to the pK_a value of the modulator, the addition of deprotonation reagent, the synthesis temperature, and the reactant concentrations. The modulator with lower pK_a value, the lower synthesis temperature, and the higher reactant concentrations lead to more MC defects. The formation of ML defects and MC defects caused significant pore size variation of the UiO-66 framework. The pore size distribution of synthesized samples allows us to track the variation of both ML and MC defects. These large cavities allow the deposition of large molecules in the framework to combine the benefits of the large surface area of MOFs and functionality of the deposited molecules. Ferrocene was incorporated into the defective UiO-66 framework using the CVD method. Nitrogen adsorption and pore size distributions verified that the ferrocene was incorporated mostly into MC defective sites.

■ ASSOCIATED CONTENT

Supporting Information

The Supporting Information is available free of charge on the ACS Publications website at DOI: 10.1021/acs.iecr.8b03516.

Sample processing, characterizations, computation studies, and a portion of the characterization results (PDF)

■ AUTHOR INFORMATION

Corresponding Author

*E-mail: bmu@asu.edu.

ORCID

Bohan Shan: 0000-0001-5674-981X

Bin Mu: 0000-0002-9117-1299

Author Contributions

[†]B.S. and S.M. contributed equally and are co-first authors.

Notes

The authors declare no competing financial interest.

■ ACKNOWLEDGMENTS

We gratefully acknowledge the National Science Foundation (Grant Number CBET-1748641 and CMMI-1825594). We gratefully acknowledge the use of facilities within the Leroy Eyring Center for Solid State Science at Arizona State University and ASU SEMTE lab manager Fred Pena for continued support. We also appreciate that Dr. Lenore Dai provided the TGA analyzer and Yifei Xu and Wendy Lin for the technical support.

■ REFERENCES

- (1) Liu, Y.; Wang, Z. U.; Zhou, H.-C. Recent Advances in Carbon Dioxide Capture with Metal-Organic Frameworks. *Greenhouse Gases: Sci. Technol.* **2012**, *2* (4), 239–259.
- (2) Li, J. R.; Sculley, J.; Zhou, H. C. Metal-Organic Frameworks for Separations. *Chem. Rev.* **2012**, *112*, 869–932.
- (3) Ma, S. Q.; Zhou, H. C. Gas Storage in Porous Metal-Organic Frameworks for Clean Energy Applications. *Chem. Commun.* **2010**, *46* (1), 44–53.
- (4) Wang, L.; Han, Y.; Feng, X.; Zhou, J.; Qi, P.; Wang, B. Metal-Organic Frameworks for Energy Storage: Batteries and Supercapacitors. *Coord. Chem. Rev.* **2016**, *307*, 361–381.
- (5) Huang, Y.-B.; Liang, J.; Wang, X.-S.; Cao, R. Multifunctional Metal-organic Framework Catalysts: Synergistic Catalysis and Tandem Reactions. *Chem. Soc. Rev.* **2017**, *46* (1), 126–157.

(6) Hu, Z.; Deibert, B. J.; Li, J. Luminescent Metal-Organic Frameworks for Chemical Sensing and Explosive Detection. *Chem. Soc. Rev.* **2014**, *43* (16), 5815–5840.

(7) Kreno, L. E.; Leong, K.; Farha, O. K.; Allendorf, M.; Van Duyne, R. P.; Hupp, J. T. Metal-Organic Framework Materials as Chemical Sensors. *Chem. Rev.* **2012**, *112* (2), 1105–1125.

(8) DeCoste, J. B.; Peterson, G. W.; Jasuja, H.; Glover, T. G.; Huang, Y.; Walton, K. S. Stability and Degradation Mechanisms of Metal-organic Frameworks Containing the Zr₆O₄(OH)₄ Secondary Building Unit. *J. Mater. Chem. A* **2013**, *1* (18), 5642.

(9) Valenzano, L.; Civalieri, B.; Chavan, S.; Bordiga, S.; Nilsen, M. H.; Jakobsen, S.; Lillerud, K. P.; Lamberti, C. Disclosing the Complex Structure of UiO-66 Metal Organic Framework: A Synergic Combination of Experiment and Theory. *Chem. Mater.* **2011**, *23* (7), 1700–1718.

(10) Cavka, J. H.; Jakobsen, S.; Olsbye, U.; Guillou, N.; Lamberti, C.; Bordiga, S.; Lillerud, K. P. A New Zirconium Inorganic Building Brick Forming Metal Organic Frameworks with Exceptional Stability. *J. Am. Chem. Soc.* **2008**, *130* (42), 13850–13851.

(11) Chavan, S.; Vitillo, J. G.; Gianolio, D.; Zavorotynska, O.; Civalieri, B.; Jakobsen, S.; Nilsen, M. H.; Valenzano, L.; Lamberti, C.; Lillerud, K. P.; et al. H₂ Storage in Isostructural UiO-67 and UiO-66 MOFs. *Phys. Chem. Chem. Phys.* **2012**, *14* (5), 1614–1626.

(12) Feng, D.; Gu, Z.-Y.; Li, J.-R.; Jiang, H.-L.; Wei, Z.; Zhou, H.-C. Zirconium-Metalloporphyrin PCN-222: Mesoporous Metal-Organic Frameworks with Ultrahigh Stability as Biomimetic Catalysts. *Angew. Chem., Int. Ed.* **2012**, *51* (41), 10307–10310.

(13) Silva, C. G.; Luz, I.; Llabres i Xamena, F. X.; Corma, A.; Garcia, H. Water Stable Zr-Benzenedicarboxylate Metal-Organic Frameworks as Photocatalysts for Hydrogen Generation. *Chem. - Eur. J.* **2010**, *16* (36), 11133–11138.

(14) Pearson, G. Hard and Soft Acids and Bases. *J. Am. Chem. Soc.* **1963**, *85* (22), 3533–3539.

(15) Feng, D.; Wang, K.; Wei, Z.; Chen, Y.-P.; Simon, C. M.; Arvapally, R. K.; Martin, R. L.; Bosch, M.; Liu, T.-F.; Fordham, S.; et al. Kinetically Tuned Dimensional Augmentation as a Versatile Synthetic Route towards Robust Metal-organic Frameworks. *Nat. Commun.* **2014**, *5*, 5723.

(16) Burtch, N. C.; Jasuja, H.; Walton, K. S. Water Stability and Adsorption in Metal-Organic Frameworks. *Chem. Rev.* **2014**, *114*, 10575–10612.

(17) Shearer, G. C.; Vitillo, J. G.; Bordiga, S.; Svelle, S.; Olsbye, U.; Lillerud, K. P. Functionalizing the Defects: Postsynthetic Ligand Exchange in the Metal Organic Framework UiO-66. *Chem. Mater.* **2016**, *28* (20), 7190–7193.

(18) Wu, H.; Chua, Y. S.; Krungleviciute, V.; Tyagi, M.; Chen, P.; Yildirim, T.; Zhou, W. Unusual and Highly Tunable Missing-Linker Defects in Zirconium Metal-Organic Framework UiO-66 and Their Important Effects on Gas Adsorption. *J. Am. Chem. Soc.* **2013**, *135* (28), 10525–10532.

(19) Ghosh, P.; Colón, Y. J.; Snurr, R. Q. Water Adsorption in UiO-66: The Importance of Defects. *Chem. Commun.* **2014**, *50*, 11329–11331.

(20) Bácia, P. S.; Guimarães, D.; Mendes, P. A. P.; Silva, J. A. C.; Guillerm, V.; Chevreau, H.; Serre, C.; Rodrigues, A. E. Reverse Shape Selectivity in the Adsorption of Hexane and Xylene Isomers in MOF UiO-66. *Microporous Mesoporous Mater.* **2011**, *139* (1–3), 67–73.

(21) Liang, W.; Coghlan, C. J.; Ragon, F.; Rubio-Martinez, M.; D'Alessandro, D. M.; Babarao, R. Defect Engineering of UiO-66 for CO₂ and H₂O Uptake – a Combined Experimental and Simulation Study. *Dalt. Trans.* **2016**, *45* (11), 4496–4500.

(22) Vermoortele, F.; Bueken, B.; Van De Voorde, B.; Vandichel, M.; Houthoofd, K.; Vimont, A.; Daturi, M.; Waroquier, M.; Van Speybroeck, V.; Kirschhock, C. E.; et al. Synthesis Modulation as a Tool to Increase the Catalytic Activity of MOFs: The Unique Case of UiO-66 (Zr). *J. Am. Chem. Soc.* **2013**, *135*, 11465–11468.

(23) Shearer, G. C.; Chavan, S.; Ethiraj, J.; Vitillo, J. G.; Svelle, S.; Olsbye, U.; Lamberti, C.; Bordiga, S.; Lillerud, K. P. Tuned to

Perfection: Ironing out the Defects in Metal-Organic Framework UiO-66. *Chem. Mater.* **2014**, *26* (14), 4068–4071.

(24) Cliffe, M. J.; Wan, W.; Zou, X.; Chater, P. a; Kleppe, A. K.; Tucker, M. G.; Wilhelm, H.; Funnell, N. P.; Coudert, F.-X.; Goodwin, A. L. Correlated Defect Nanoregions in a Metal–organic Framework. *Nat. Commun.* **2014**, *5* (May), 4176.

(25) Luz, I.; Rösler, C.; Epp, K.; Llabrés I Xamena, F. X.; Fischer, R. A. Pd@UiO-66-Type MOFs Prepared by Chemical Vapor Infiltration as Shape-Selective Hydrogenation Catalysts. *Eur. J. Inorg. Chem.* **2015**, *2015* (23), 3904–3912.

(26) Dubbeldam, D.; Calero, S.; Ellis, D. E.; Snurr, R. Q. RASPA: Molecular Simulation Software for Adsorption and Diffusion in Flexible Nanoporous Materials. *Mol. Simul.* **2015**, *7022* (September), 1–21.

(27) Dubbeldam, D.; Calero, S.; Ellis, D. E.; Snurr, R. Q. RASPA: Molecular Simulation Software for Adsorption and Diffusion in Flexible Nanoporous Materials. *Mol. Simul.* **2016**, *42* (2), 81–101.

(28) Gelb, L. D.; Gubbins, K. E. Pore Size Distributions in Porous Glasses: A Computer Simulation Study. *Langmuir* **1999**, *15* (2), 305–308.

(29) Wißmann, G.; Schaate, A.; Lilienthal, S.; Bremer, I.; Schneider, A. M.; Behrens, P. Modulated Synthesis of Zr-Fumarate MOF. *Microporous Mesoporous Mater.* **2012**, *152*, 64–70.

(30) Tsuruoka, T.; Furukawa, S.; Takashima, Y.; Yoshida, K.; Isoda, S.; Kitagawa, S. Nanoporous Nanorods Fabricated by Coordination Modulation and Oriented Attachment Growth. *Angew. Chem., Int. Ed.* **2009**, *48* (26), 4739–4743.

(31) Umemura, A.; Diring, S.; Furukawa, S.; Uehara, H.; Tsuruoka, T.; Kitagawa, S. Morphology Design of Porous Coordination Polymer Crystals by Coordination Modulation. *J. Am. Chem. Soc.* **2011**, *133* (39), 15506–15513.

(32) Shearer, G. C.; Chavan, S.; Bordiga, S.; Svelle, S.; Olsbye, U.; Lillerud, K. P. Defect Engineering: Tuning the Porosity and Composition of the Metal-Organic Framework UiO-66 via Modulated Synthesis. *Chem. Mater.* **2016**, *28* (11), 3749–3761.

(33) Ragon, F.; Horcajada, P.; Chevreau, H.; Hwang, Y. K.; Lee, U. H.; Miller, S. R.; Devic, T.; Chang, J. S.; Serre, C. In Situ Energy-Dispersive X-Ray Diffraction for the Synthesis Optimization and Scale-up of the Porous Zirconium Terephthalate UiO-66. *Inorg. Chem.* **2014**, *53* (5), 2491–2500.

(34) Li, N.; Xu, J.; Feng, R.; Hu, T.-L.; Bu, X.-H. Governing Metal–organic Frameworks towards High Stability. *Chem. Commun.* **2016**, *52* (55), 8501–8513.

(35) Shan, B.; James, J. B.; Armstrong, M. R.; Close, E. C.; Letham, P. A.; Nikkhah, K.; Lin, Y. S.; Mu, B. Influences of Deprotonation and Modulation on Nucleation and Growth of UiO-66: Intergrowth and Orientation. *J. Phys. Chem. C* **2018**, *122* (4), 2200–2206.

(36) Lu, H.; Zhu, S. Interfacial Synthesis of Free-Standing Metal-Organic Framework Membranes. *Eur. J. Inorg. Chem.* **2013**, *2013* (No. 8), 1294–1300.

(37) Zahn, G.; Zerner, P.; Lippke, J.; Kempf, F. L.; Lilienthal, S.; Schröder, C. A.; Schneider, A. M.; Behrens, P. Insight into the Mechanism of Modulated Syntheses: In Situ Synchrotron Diffraction Studies on the Formation of Zr-Fumarate MOF. *CrystEngComm* **2014**, *16* (39), 9198–9207.

(38) Zacher, D.; Liu, J.; Huber, K.; Fischer, R. A. Nanocrystals of [Cu₃(btc)₂] (HKUST-1): A Combined Time-Resolved Light Scattering and Scanning Electron Microscopy Study. *Chem. Commun.* **2009**, *3* (9), 1031–1033.

(39) Zhao, Y.; Zhang, Q.; Li, Y.; Zhang, R.; Lu, G. Large-Scale Synthesis of Monodisperse UiO-66 Crystals with Tunable Sizes and Missing Linker Defects via Acid/Base Co-Modulation. *ACS Appl. Mater. Interfaces* **2017**, *9*, 15079.

(40) McIntyre, S. M.; Shan, B.; Wang, R.; Zhong, C.; Liu, J.; Mu, B. Monte Carlo Simulations to Examine the Role of Pore Structure on Ambient Air Separation in Metal–Organic Frameworks. *Ind. Eng. Chem. Res.* **2018**, *57* (28), 9240–9253.

(41) Zhang, W.; Banerjee, D.; Liu, J.; Schaef, H. T.; Crum, J. V.; Fernandez, C. A.; Kukkadapu, R. K.; Nie, Z.; Nune, S. K.; Motkuri, R.

K.; et al. Redox-Active Metal-Organic Composites for Highly Selective Oxygen Separation Applications. *Adv. Mater.* **2016**, *28* (18), 3572–3577.